Molecular Biotechnology (2024) 66:737–755
https://doi.org/10.1007/s12033-023-00685-3

ORIGINAL PAPER

Scaffold Hopping and Screening for Potent Small Molecule Agonists for GRP94: Implications to Alleviate ER Stress-Associated Pathogenesis

Shoufia Jabeen Mubarak[1] · Surabhi Gupta[2] · Hemamalini Vedagiri[1]

Received: 30 September 2022 / Accepted: 27 January 2023 / Published online: 10 February 2023

Abstract

Disparity in the activity of Endoplasmic reticulum (ER) leads to degenerative diseases, mainly associated with protein misfolding and aggregation leading to cellular dysfunction and damage, ultimately contributing to ER stress. ER stress activates the complex network of Unfolded Protein Response (UPR) signaling pathways mediated by transmembrane proteins IRE1, ATF6, and PERK. In addition to UPR, many ER chaperones have evolved to optimize the output of properly folded secretory and membrane proteins. Glucose-regulated protein 94 (GRP94), an ER chaperone of heat shock protein HSP90 family, directs protein folding through interaction with other components of the ER protein folding machinery and assists in ER-associated degradation (ERAD). Activation of GRP94 would increase the efficacy of protein folding machinery and regulate the UPR pathway toward homeostasis. The present study aims to screen for novel agonists for GRP94 based on Core hopping, pharmacophore hypothesis, 3D-QSAR, and virtual screening with small-molecule compound libraries in order to improve the efficiency of native protein folding by enhancing GRP94 chaperone activity, therefore to reduce protein misfolding and aggregation. In this study, we have employed the strategy of small molecule-dependent ER programming to enhance the chaperone activity of GRP94 through scaffold hopping-based screening approach to identify specific GRP94 agonists. New scaffolds generated by altering the cores of NECA, the known GRP94 agonist, were validated by employing pharmacophore hypothesis testing, 3D-QSAR modeling, and molecular dynamics simulations. This facilitated the identification of small molecules to improve the efficiency of native protein folding by enhancing GRP94 activity. High-throughput virtual screening of the selected pharmacophore hypothesis against Selleckchem and ZINC databases retrieved a total of 2,27,081 compounds. Further analysis on docking and ADMET properties revealed Epimedin A, Narcissoside, Eriocitrin 1,2,3,4,6-O-Pentagalloylglucose, Secoisolariciresinol diglucoside, ZINC92952357, ZINC67650204, and ZINC72457930 as potential lead molecules. The stability and interaction of these small molecules were far better than the known agonist, NECA indicating their efficacy in selectively alleviating ER stress-associated pathogenesis. These results substantiate the fact that small molecule-dependent ER reprogramming would activate the ER chaperones and therefore reduce the protein misfolding as well as aggregation associated with ER stress in order to restore cellular homeostasis.

Keywords ER stress · UPR · GRP94 · Scaffold hopping · Pharmacophore modeling · 3D-QSAR · MD simulations

Abbreviations

ER	Endoplasmic reticulum
UPR	Unfolded protein response
IRE1	Inositol-requiring ER-to-nucleus signal kinase 1
PERK	Protein kinase-like ER kinase
GRP94	Glucose-regulated protein 94
QSAR	Quantitative structure–activity relationship
MD	Molecular dynamics
RMSD	Root mean square deviation
RMSF	Root mean square fluctuation
ROS	Reactive oxygen species
ADMET	Absorption, distribution, metabolism, excretion, and toxicity
MDCK	Madin–Darby canine kidney cells
fs	Femtosecond
ns	Nanosecond

✉ Hemamalini Vedagiri
hemamalini@buc.edu.in

[1] Department of Bioinformatics, Bharathiar University, Coimbatore, Tamil Nadu, India

[2] Department of Reproductive Biology, All India Institute of Medical Sciences, Ansari Nagar, New Delhi 110029, India

Introduction

Endoplasmic reticulum (ER) is a basic sub-cellular compartment responsible for the critical process involving folding and maturation of the proteome, primarily transmembrane and secreted proteins in eukaryotic cells. ER protein homeostasis is highly sensitive to changes in intracellular and extracellular stimuli, involving a complex network of regulators including chaperones, ensuring high degrees of fidelity and efficiency. Nevertheless, alteration in the protein-folding environment causes accumulation of misfolded proteins profoundly inducing ER stress, which subsequently activates the Unfolded Protein Response (UPR) constituted by three signaling pathways mediated by downstream ER stress sensors IRE1 (the inositol-requiring ER-to-nucleus signal kinase 1), PERK (protein kinase-like ER kinase), and ATF6 (Activating Transcription Factor6) [1, 2]. This UPR pathway leads to a series of downstream events like decreasing translation and increasing transcription of ER chaperones to restore normal cellular function and survival [3]. However in chronic ER stress, protective remodeling does not happen due to prolonged UPR activation ultimately leading to pro-apoptotic signals that eventually eliminate the stressed cells [4].

The major role of UPR is to re-establish homeostasis either by increasing folding capacity via expression of folding chaperones or by the downregulation of ER protein client load via inhibiting protein translation and promoting the degradation of misfolding proteins. Accumulating experimental and substantial clinical evidence suggests that prolonged ER stress crucially impact the pathogenesis of various human diseases, including diabetes, cardiovascular diseases, inflammatory diseases, neurodegenerative disorders, and cancer. Currently, cellular ER stress along with oxidative stress in many disease conditions is treated with the administration of antioxidants and chemical chaperones. However, their protective effects are not sustainable, hence altering the molecular machinery of the cell will provide ways to understand the underlying metabolic changes. Interestingly, transcriptionally reprogramming of ER proteostasis network would augment ER protein-folding capacity by modulating the UPR downstream signaling pathways and therefore prevent protein aggregation and misfolding [5–9].

Heat shock protein 90 (Hsp90) is a evolutionarily conserved, ubiquitous family of ATP-dependent molecular chaperone that plays essential role in stabilizing protein folding, to modulating cellular signaling by regulating many client protein substrates. In eukaryotes, HSP90 exists as four isoforms: cytosolic HSP90α and HSP90β, ER-resident GRP94, and tumor necrosis factor receptor-associated protein 1 (TRAP1) which localizes to the mitochondria [10]. GRP94, the ER-resident member of the hsp90 family, governs the maintenance and activation of many essential proteins, particularly membrane-resident and secreted protein clients, namely MHC class II, integrins, and Toll-Like receptors. Coordinated up-regulation of GRP94 with many other ER folding components was first discovered while using pharmacological treatments to induce UPR [11, 12]. There are four ways to acknowledge the contribution of GRP94 in ER quality control which are (a) chaperoning the protein folding, (b) interacting with the ER protein-folding machinery, (c) storing calcium, and (d) assisting the targeting of misfolded proteins to ER-associated degradation (ERAD) [13–15].

The most important activity of GRP94 subsists as molecular chaperone that directs folding and/or assembly of secreted and membrane proteins. GRP94 protein contains three domains: *C*-terminal domain with ATP-binding site thought to regulate HSP90 homodimerization, charged middle linker region, and an *N*-terminal domain that contains an ATP-binding pocket (with ATPase activity) which regulates the turnover of folded client proteins (Fig. 1). Both the *C*- and *N*-terminal ATP-binding sites have been greatly explored as target for inhibitors; however, the majority of HSP90 inhibitors have concentrated only on the *N*-terminal ATP-binding site [16, 17]. Molecular chaperones require ATP hydrolysis to favor the native folding of their substrates, to avoid aggregation, and revert protein misfolding. GRP94, an ER chaperone displays selective ligand binding affinity to NECA (5′-*N*-ethylcarboxamido adenosine), a broad-spectrum adenosine A2 receptor agonist which is more potent than adenosine and a well-known activator of GRP94. Several structural studies have demarcated the interaction of NECA with the *N*-terminal region of GRP94. A number of studies indicate that scaffolds generated from core hopping of known agonist with further pharmacophore modeling and QSAR validations will provide similar scaffold and ligands which would serve as potential agonist in activating the target [23]. Therefore, we decipher that NECA would probably increase the chaperone activity of GRP94.

A number of small-molecule pharmacological chaperones have emerged as a novel therapeutic approach to treat metabolic disorders, such as type 2 diabetes and neurodegenerative diseases. Small-molecule kinase inhibitors and ATP mimetics have shown to activate the IRE1 arm of the UPR signaling pathway and reduce ER stress-associated pathogenesis. Hence, identification of small molecules that enhance the ER chaperoning activity and preferentially activation of the UPR-associated transcriptional program is needed to ameliorate protein misfolding and aggregation. This strategy of small molecule-dependent ER programming would restore the protein-folding ability of GRP94 thereby preventing ER stress-induced disease pathogenesis [18, 19]. With this insight, we have employed Scaffold hopping,

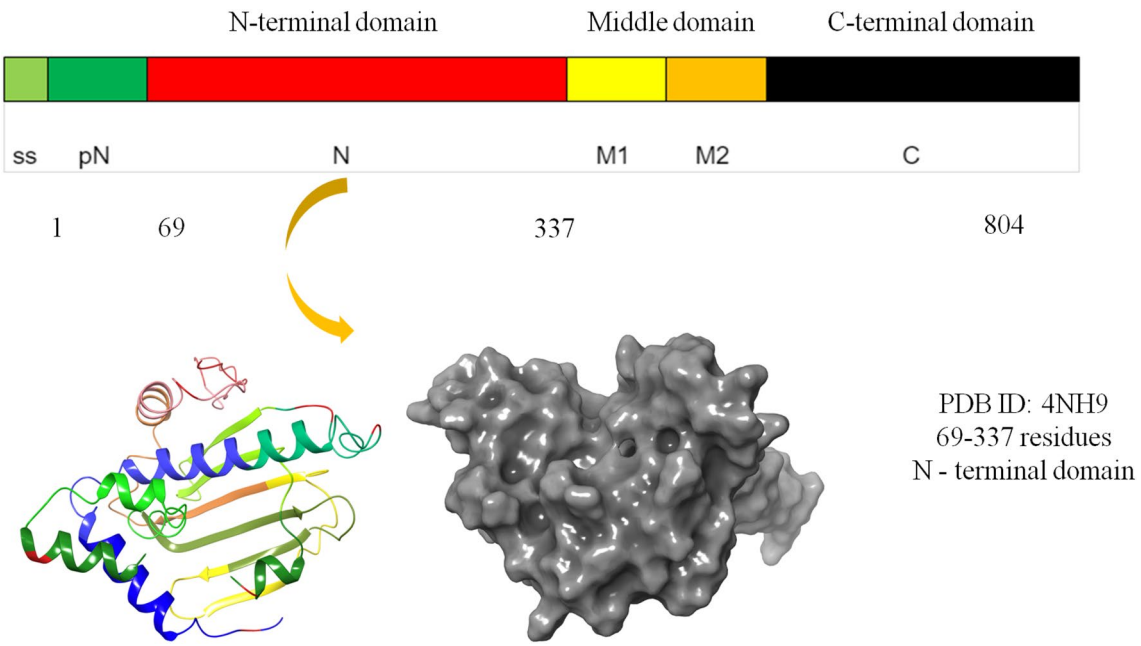

Fig. 1 GRP94 protein with three distinct domains showing the Adenosine binding N-terminal domain (69-337 region)

pharmacophore modeling, QSAR-based virtual screening, molecular docking, and dynamic simulations to screen small molecules as potential agonists for GRP94 using NECA scaffold.

Materials and Methods

Protein and Ligand Preparation

The crystal structure of GRP94 was downloaded from the Protein Data Bank (PDB ID: 4NH9, https://www.rcsb.org/) with resolution 2.77 Å [20]. All the water molecules were removed, hydrogen atoms were added, and the H-bond assignment was optimized with exhaustive sampling using Glide module of Schrödinger Maestro Suite 2018-4 version 11.8, https://www.schrodinger.com/products/maestro). Finally, the protein structure was energy minimized using the OPLS3e force field to reach the converged root mean square deviation (RMSD) of 0.30 Å. The grid box was defined using "Receptor Grid Generation" by assigning a common constituency point from where a cubic grid box was extended to touch the bounty of 20 Å in size. Ligprep module of Schrodinger Maestro was used to prepare the 3D co-ordinates of the retrieved ligand structures from the selected ZINC and Selleckchem compound databases [21]. The ligands were geometrically minimized using the OPLS3e force field with the Truncated Newton Conjugate Gradient of RMSD below 0.01 kJ/Å. Eventually, the minimized conformer was filtered through a relative energy window of 10 kcal/mol and a minimum atom deviation of 1.00 Å. The ionization states were created for ligands at a physiological pH of 7.2 ± 0.2 and all other variables remained default. The tautomers of the ligands were generated, optimized, and partial atomic charges were computed using the OPLS3e force field [22]. Then the prepared ligands structures were segregated and selected by removing the repetitive compounds manually.

Core Hopping of NECA

Core Hopping v2.1 module of Schrodinger Maestro 11.8 software was used to modify the known agonist by performing fragment-based replacement using ligand- and isosteric-based constraints. The first step was to define the points at which the cores were attached to the scaffold using Define Combinations mode. Next step was to subject the scaffold for optimization process for altering the cores. The altered scaffolds were selected based on the template of NECA and were considered as the initial structure for further analysis. The selected scaffolds of NECA with new analogs were further subjected for Pharmacophore modeling, 3D-QSAR, virtual screening, and molecular dynamics simulations. This parameter is based on the principle of bio-isosteres by replacing functional groups in the template ligand, for targeting and reducing the toxic side effects as well as improving the curative effects [23, 24].

Pharmacophore Generation and Modeling

Pharmacophore models were generated by ligand-based modeling through PHASE module 11.8 of Schrödinger Maestro 2018. Phase allows specification of matching chemical molecules and marginalization for pharmacophore features. The common pharmacophoric features were used for generating the hypothesis. The box size was adjusted to 2 Å with default scoring parameters and the maximum number of sites was set to 5 and minimum to 3. The top ranking hypothesis was selected for further screening. The common integral pharmacological features involved were hydrogen bond acceptor (A), hydrogen bond donor (D), hydrophobic group (H), and aromatic ring (R). After the pharmacophore generation, the scoring function was used to analyze the hypothesis. The selected alignment was computed using the default values and survival score. The feature definitions were utilized to map the positions of pharmacophore sites and were represented internally by a set of SMARTS patterns [25]. To encompass the space occupied by the aligned training set molecules, the grid was generated. Each model contains five or more partial least square (PLS) factors that tend to suit it [26].

3D-QSAR Validation

An atom-based 3D-QSAR model was built from the alignment on the simplest pharmacophore model through PHASE 11.8. A PLS analysis, that correlated the estimated activities with the observed activities, was used to evaluate the predictive ability of the best-scoring hypotheses [27]. QSAR models were important to elucidate the structural information of the ligand's active conformation. QSAR was mainly based on known biological activities for structural and functional ligands for the pharmacophore model [28]. The statistical parameters such as R^2 (coefficient of determination), SD (standard deviation of regression), and Q^2 (cross-validated coefficient) were calculated to assess the general significance of the model [29].

Virtual Screening and Docking

Virtual screening was performed in ZincPharmer (http://zincpharmer.csb.pitt.edu/) and Selleckchem Natural Compound library with 2726 compounds (https://www.selleckchem. com/screening/natural-product-library.html) by exploiting the best pharmacophore model to efficiently search the datasets for fixed conformers [30, 31]. Low-energy 3D conformers with the best bond lengths and angles were generated for each two-dimensional structure. In this study, ADHR_2 was the best hypothesis based on which query search was performed to identify hits matching the pharmacophoric features of the hypothesis using the search for match option in PHASE. The default constraints included a maximum of 0.7 Root Mean Square Deviation (RMSD), obeying 10 rotatable bond cutoffs, with a molecular weight range of 180–500 Da. The obtained database hits were ranked depending on the degree of consistency with the pharmacophore model. A minimum fit value of > 3, the lowest limit to qualify as a hit compound, was applied to decrease the number of hits. Molecules with good fitness scores were selected for further docking studies.

Structure-based docking studies were carried out to investigate the intermolecular interactions between the ligand and the targeted protein using Glide 11.8, Schrodinger, 2018. In the first step, the high-throughput virtual screening mode of Glide was employed and 10% of the top-scoring ligands were further subjected to Glide SP docking. Again, 10% of the top-scoring leads from Glide SP were retained and all the ligands were subjected further to Glide XP docking. Low-energy conformations of all the compounds were docked into the active site of GRP94 using Grid-based Ligand Docking with Energetics [32] in extra precision mode without applying any constraint. The best-docked structure was identified using Glide score function, Glide energy, and Glide E model energy. The top ten lead compounds were selected based on their docking score for further studies.

Lipinski's Rule and ADMET Prediction

Qikprop v.11.8, module was applied to screen the lead compounds for their ADMET properties. ADMET gives the specific range for analyzing the drug-like properties, such as aqueous solubility (QPlog S), brain/blood partition coefficient (QP log BB), (QP log Po/w), predicted apparent MDCK cell permeability (QPMDCK), and human oral absorption [33]. The drug-like behavior of the compounds was predicted through the analysis of pharmacokinetic profile of the compounds. Physically significant descriptors and pharmaceutically relevant properties of all the test compounds such as molecular weight, log *P*, H-bond donors, and H-bond acceptors were analyzed in accordance with Lipinski's rule of five [34]. Finally the selected compounds were filtered through Lipinski's rule to ensure the properties of pharmacokinetics.

SwissADME online tool (http://www.swissadme.ch/) brings together the most relevant computational methodologies to give a worldwide assessment of small-molecule pharmacokinetics profiles [35]. The pharmacological properties of the top lead molecules were assessed based on different parameters and the bioavailability radar was generated.

Molecular Dynamics Simulations

The best-docked complex of GRP94 target protein acquired from the virtual screening result was explored for the

conformational stability using molecular dynamic (MD) simulations. MD simulations were carried out using the Desmond module of Schrodinger suite of 2018-4 for 100 ns with the force field OPLS-2005. The generated MD trajectory files were examined in order to determine the equilibrium of dynamics over the period of time. The structure was generated and solvated using the TIP4P model by orthorhombic water box parameters as well as neutralizing with counter ions from each edge of the box [36]. Before the MD simulations, the complex charge was electrically neutralized as well as the system was minimized with their energies by series of heating and equilibrium processes. The selected complexes were energy minimized by the protocol of steepest descent minimization for the maximum extent followed by a cascade of molecular simulations. The above mentioned steps were taken into account at temperature of 300 K with a NVT ensemble by Nose–Hoover thermostats, whereas the pressure was maintained using Berendsen thermostats method [37]. Eventually the salt concentration of the system was set in a specified state as 0.15-M Na^+/Cl^- for the neutralizing components in a dynamics system. The process of simulated protein–ligand complexes were examined to assess the root mean square deviations (RMSD) for the MD trajectory frames of the selected simulated structure [38]. Further, RMSD variations were calculated and the Root mean square fluctuation (RMSF) was analyzed to study the structural changes of both the GRP94 protein and ligand complexes.

Results

In the present study, novel GRP94 agonists were designed and identified by means of core hopping approach, the structure of NECA (5′-*N*-ethylcarboxamidoadenosine), the known agonist for GRP94 was used as the lead compound. The newly designed scaffolds of GRP94 from core hopping analysis [39] were subjected to pharmacophore hypothesis testing, 3D-QSAR model validations, and high-throughput virtual screening using Selleckchem and ZINCpharmer database to effectively identify small molecules for enhancing GRP94 activity. The screened compounds were validated as effective drug molecules based on ADMET prediction and the top lead compounds were taken over for further analysis. Molecular dynamics simulations of the representative ZINC and Selleckchem compounds with GRP94 protein were also performed to study the binding stability of the protein–ligand complexes.

Core Hopping Approach

The scaffold structure of NECA was divided into three parts as Core A, Core B-linkers, and Core C. The linkers and core of NECA were modified to produce various novel scaffolds. After optimization, 37 novel ligand-based scaffolds were generated by Core hopping. The newly constructed scaffolds obtained by modifying the linkers were visually inspected and four new scaffolds were selected for further analysis (Fig. 2). These scaffolds were then subjected for pharmacophore modeling, QSAR analysis, and virtual screening.

Pharmacophore Model Generation

The pharmacophore models were generated using a set of pharmacophore features in order to get suitable sites for all the new scaffolds. In total, 392 common pharmacophore hypotheses were generated using different combinations of 13 variants. Among the 13 variants, five pharmacophore models ADHH_1, ADHHR_3, ADHR_2, DHHR_1, and DHHR_4 were selected for further analysis (Table 1). The scoring procedure provides a ranking of the different hypotheses, allowing us to make rational choices. The scoring algorithm includes the alignment of site points and vectors, volume overlap, number of ligands matched, selectivity, relative conformational energy, and activity [40]. A total of five hypotheses survived the scoring processes were utilized to build an atom-based QSAR model. In the present study, the pharmacophore site of the selected scaffold was defined by a set of four pharmacophoric features: hydrogen bond acceptor (A), hydrogen bond donor (D), hydrophobic groups (H), and an aromatic ring (R). Hypothesis ADHR_2 was selected as the best hypothesis based on highest survival score of 4.594 and volume of around 0.640 (Fig. 3).

Evaluation of 3D-QSAR

The 3D-QSAR model prediction and validation were performed for the five selected pharmacophore hypothesis [38]. Regression values for the QSAR model were analyzed with the increasing number of PLS factors as the statistical significance and predictive ability of the model also incrementally increased up to 7. ADHR_2 has the most significant R^2 value of 0.3170, predictive power Q^2 value of 0.1039, Pearson R value of 0.3483, variance (SD) of 1.2098 indicative of its best fit, and high cross-validated coefficient of correlation (Table 2). In addition, ADHR_2 has P-value of $8.73e^{-018}$ indicative of the goodness of the model (Fig. 3).

Virtual Screening

Structure-based docking studies were carried out to investigate the intermolecular interaction between the ligands and the targeted protein, GRP94 using Glide [41]. ADHR_2 hypothesis was subjected for virtual screening against ZINC and Selleckchem databases to obtain ligands that match the pharmacophoric features of the

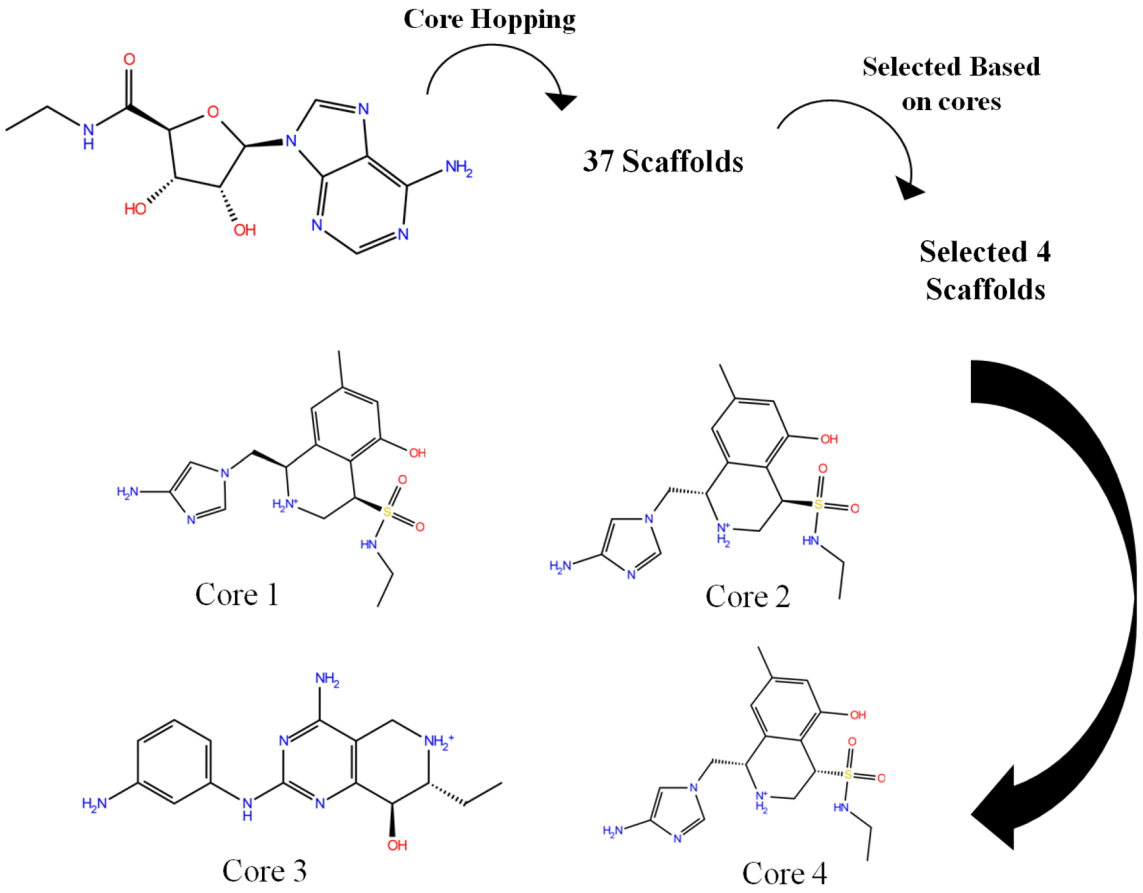

Fig. 2 Scaffolds generated by Core hopping of NECA

Table 1 Pharmacophore hypothesis generated for the NECA scaffolds

Hypothesis ID	Survival score	Survival inactive score	Adjusted score	Site	Vector	Volume	Matches
ADHH_1	4.232	1.941	2.291	0.404	0.852	0.455	4
ADHHR_3	4.581	1.890	2.691	0.262	0.827	0.444	5
ADHR_2	**4.594**	**1.184**	**3.014**	**0.668**	**0.930**	**0.640**	**4**
DHHR_1	4.577	1.942	2.309	0.522	0.825	0.415	4
DHHR_4	4.425	1.411	2.636	0.479	0.833	0.358	4

Bold values indicate the ligands that were selected for further analysis and the score based on which selection was made

model. A total of 2, 26, 248 compounds from ZincPharmer database and 833 compounds from Selleckchem were retrieved as hits. These hit compounds were docked onto GRP94 protein using Glide XP module of Schrodinger. The top ten ligands from ZINC database (Table 3) interacted with the following GRP94 active site residues ASN107, LYS114, ASP149, ASN162, GLY196, PHE199, and TYR200 either by hydrogen bonding or hydrophobic interactions (Fig. 4). Further, the potential lead molecules such as ZINC39737222, ZINC92952357, ZINC67650204, ZINC72457930, and ZINC15669361 had their docking score range from − 12.271 to − 9.025 which was considerably much higher than the known agonist, NECA (ZINC3995401).

Similarly, the top hits from Selleckchem database (Table 4) exhibited more interactions with GRP94 active site residues particularly, ASN107, ASP110, LYS114, ASP149, GLU158, LYS161, ASN162, GLY196, PHE199, and TYR200 either by hydrogen bonding or hydrophobic interactions (Fig. 5). In addition, the potential lead molecules

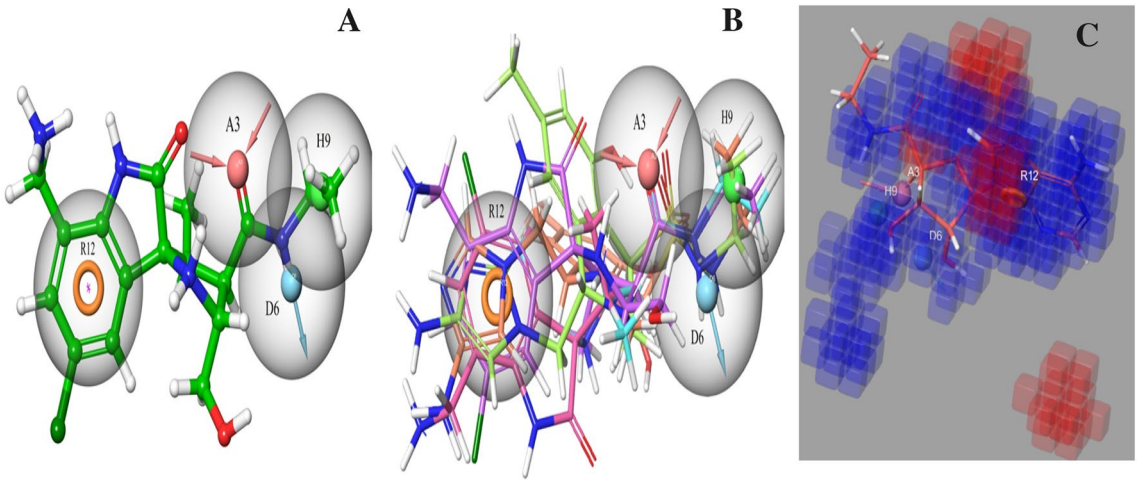

Fig. 3 **A** Structure-based Pharmacophore Mapping of ADHR_2 Hypothesis, **B** Common Pharmacophore Hypothesis aligned with all the Variants, and **C** Atom-based 3D-QSAR model Visualized for the selected Hypothesis ADHR_2

Table 2 Atom-based 3D-QSAR validation for NECA scaffolds

Hypothesis ID	SD	R^2	F	P	RMSE	Q^2	Pearson R
ADHH_1	0.8479	0.3828	59.9	$5.94e^{-016}$	1.23	0.0963	0.3342
ADHHR_3	0.8916	0.4164	27.1	$6.95e^{-006}$	1.41	0.0899	0.3195
ADHR_2	**1.2098**	**0.3170**	**90.0**	$\mathbf{8.73e^{-018}}$	**1.42**	**0.1039**	**0.3483**
DHHR_1	1.1868	0.5252	84.1	$6.35e^{-014}$	1.75	0.0479	0.2821
DHHR_4	1.2041	0.4944	86.3	$1.02e^{-026}$	1.52	0.0027	0.0367

Bold values indicate the ligands that were selected for further analysis and the score based on which selection was made

Table 3 Docking and Binding energy of top hit compounds from ZINC database with 4NH9

Lead	ZINC ID	Glide score	Glide energy	Interacting residues
	NECA	**− 6.513**	**− 28.589**	**TYR200,ASN107,ASN162**
1*	ZINC39737222	**− 12.271**	**− 49.214**	**ASN107, ASN162**
2	ZINC65393724	− 11.474	− 44.969	ASN162
3	ZINC40139446	− 11.094	− 50.302	LYS114
4	ZINC64058574	− 10.900	− 42.391	TYR200
5*	ZINC92952357	**− 10.535**	**− 40.686**	**ASP149, ASN162, ASN107**
6*	ZINC67650204	**− 10.529**	**− 32.239**	**ASN107,GLY196, PHE199, ASN162**
7	ZINC65432603	− 10.527	− 41.317	ASN162
8	ZINC65393724	− 10.507	− 42.704	ASN162
9*	ZINC72457930	**− 10.454**	**− 42.552**	**ASN162, LYS114**
10*	ZINC15669361	**− 9.025**	**− 54.002**	**ASN107, TYR200**

Bold values indicate the ligands that were selected for further analysis and the score based on which selection was made

*Top five ligands that were selected for molecular dynamics simulations

such as 1,2,3,4,6-O-Pentagalloylglucose, Epimedin A, Narcissoside, Eriocitrin, and Secoisolariciresinol diglucoside had their docking score ranging from − 14.027 to − 13.096 and Glide energy from − 75.043 to − 61.039 which was considerably significant than the known agonist, NECA (ZINC3995401).

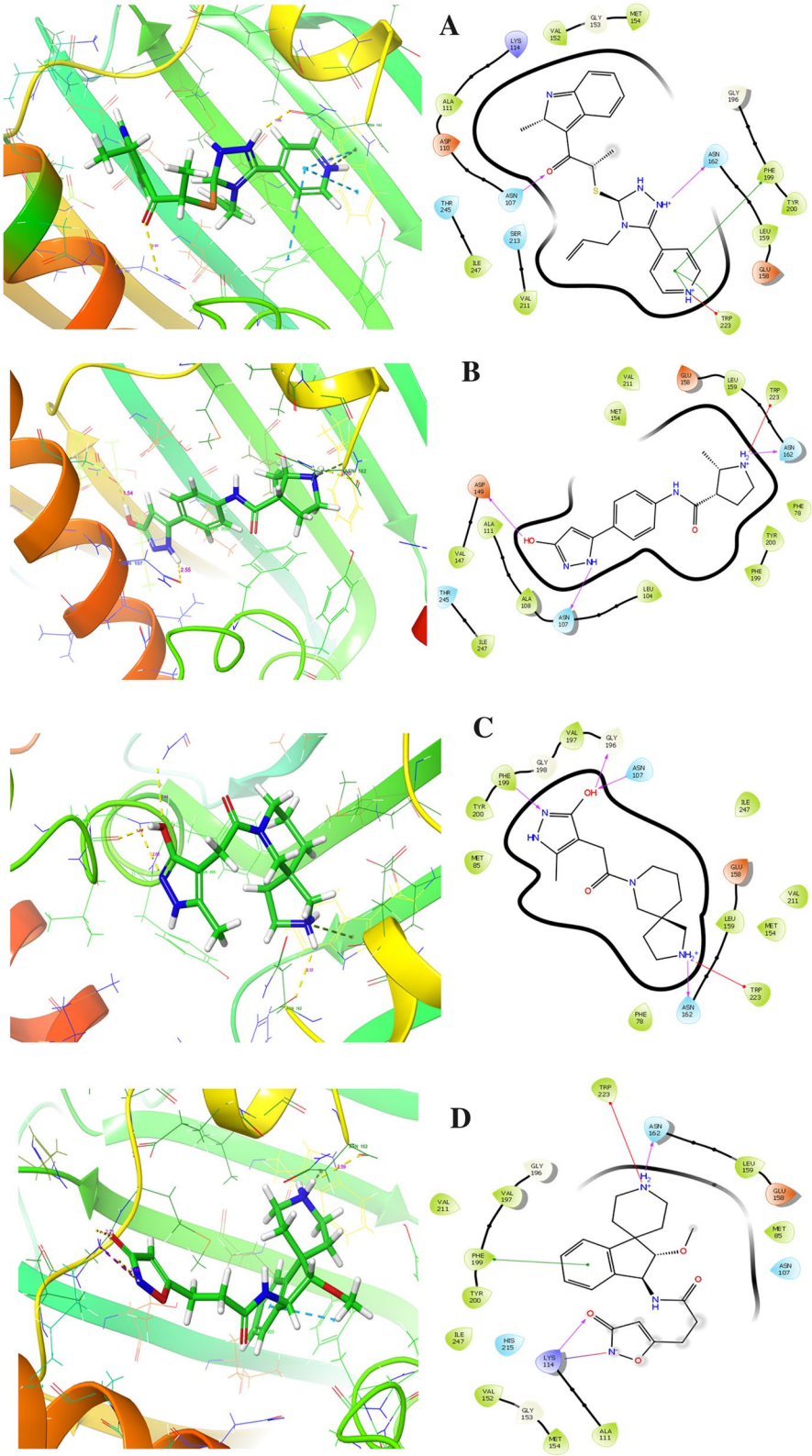

Fig. 4 2D and 3D Interactions of GRP94 and Top hit compounds from ZINCpharmer: **A** ZINC39737222, **B** ZINC92952357, **C** ZINC67650204, **D** ZINC72457930, and **E** ZINC15669361

Fig. 4 (continued)

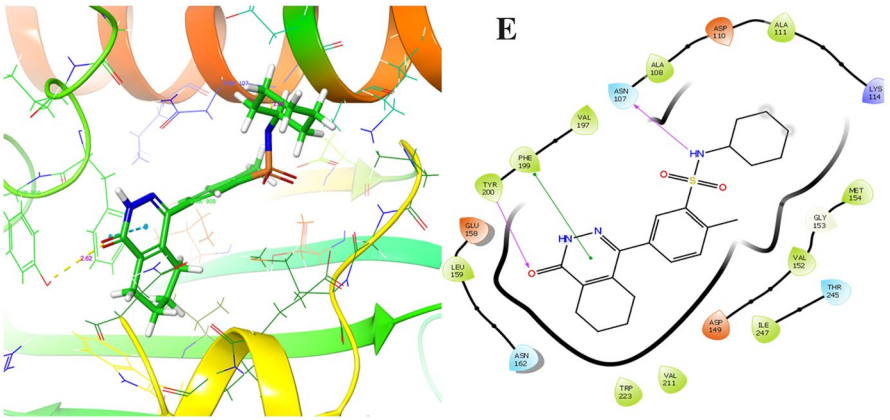

Table 4 Docking and binding energy of top hit compounds from Selleckchem database with 4NH9

Lead	Selleckchem Name	Glide Score	Glide energy	Interacting residues
0	NECA	**− 6.513**	**− 28.589**	**TYR200,ASN107,ASN162**
1	1,2,3,4,6-O-Pentagalloylglucose	− 14.027	− 75.043	ASP110,GLU158,LYS161,ASN162,PHE199(PI-PI)
2	Epimedin A	− 13.413	− 66.270	LYS161,ASN162,GLU158,LYS114,TYR200
3	Narcissoside	− 13.520	− 62.360	ASN162(3),GLU158,ASP110,ASN107,ASP149
4	Eriocitrin	− 13.195	− 64.653	ASP110,ASN107,ASN162,ASP149,PHE199
5	Secoisolariciresinol diglucoside	− 13.096	− 61.039	GLU158,LYS114,TYR200,ASP149
6	Liensinine	− 12.996	− 52.129	LYS114(PI-CAT),GLU158,ASN107,ASP110
7	Proanthocyanidins	− 12.616	− 62.105	ASP149,GLU158,PHE199
8	Neochesperidin	− 12.319	− 54.923	TY200,PHE(PI-PI),ASN162,PHE195
9	Rutin DAB 10	− 12.048	− 64.579	GLU158,LYS114
10	Boldine	− 12.021	− 38.360	GLY196,PHE(PI-PI)

Bold values indicate the ligands that were selected for further analysis and the score based on which selection was made

ADMET Analysis

Lipinski's rule of five was based on the physicochemical properties of drugs and candidate drugs in clinical trials to evaluate drug likeness. Qikprop module of Schrödinger was utilized to examine the drug likeness of compounds. The percentage of the human oral absorption of selected lead compounds was found to be 52% to 100%. For selected lead compounds ZINC39737222, ZINC92952357, ZINC67650204, ZINC72457930, and ZINC15669361, the parameters like water solubility (QPlogS), blood barrier (Qplog BB), and cell permeability (QPPCaco) were within the permissible range as depicted in Table 5. Human oral absorption was 100% for ZINC39737222, 70.531% for ZINC92952357, 58.50% for ZINC67650204 as well as ZINC72457930, and 90.153% for ZINC15669361 indicating their efficacy as potential drug molecules with good therapeutic efficiency.

The different parameters of drug-likeness analysis of the lead compounds were visualized using the SwissADME bioavailability radar (Figs. 6 and 7) [42]. Narcissoside and Eriocitrin have no pharmacokinetics interference as well as are non-inhibitors of CYP enzymes which attributes to their excellent drug-like properties with strong solubility and no excretion issues. The drug-likeness characteristics (Table 6) of Narcissoside are appropriate since they follow the Lipinski RO5 with minimal violation, zero alerts for Pan-Assay Interference Compounds (PAINS), and a bioavailability score of 0.17. Although, the potential bioactive compound Epimedin A exhibits negligible solubility, violate drug-likeness parameters because of its higher molecular weight. The drug-likeness analysis of ZINC top lead compounds using SwissADME indicated ZNC92952357 and ZINC67650204 with bioavailability score of 0.55 which signifies good pharmacokinetic properties and significant cellular permeability.

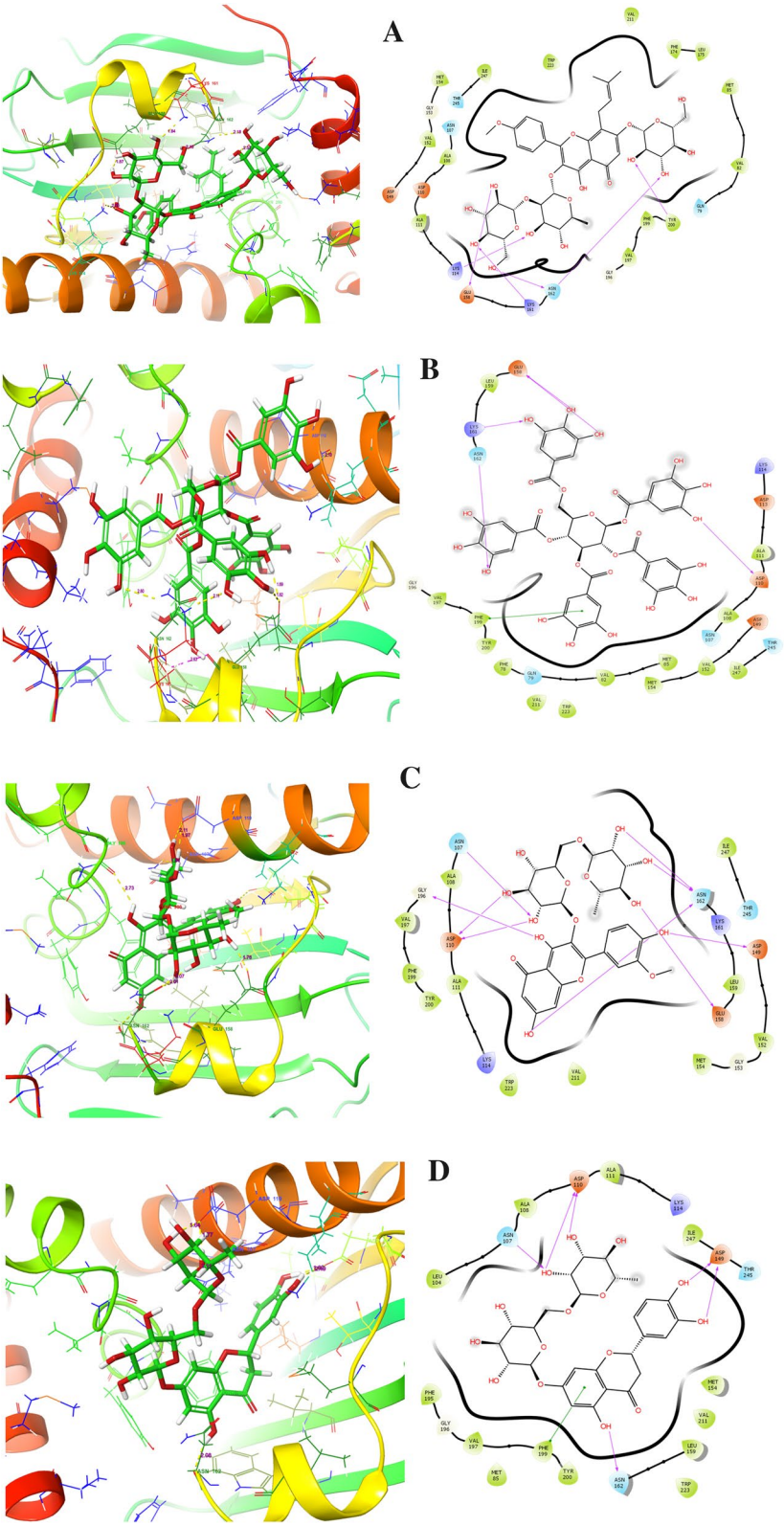

Fig. 5 2D and 3D Interactions of GRP94 and Top hit compounds from Selleckchem **A** Epimedin A, **B** 1,2,3,4,6-O-Pentagalloylglucose, **C** Narcissoside, **D** Eriocitrin, and **E** Secoisolariciresinol diglucoside

Fig. 5 (continued)

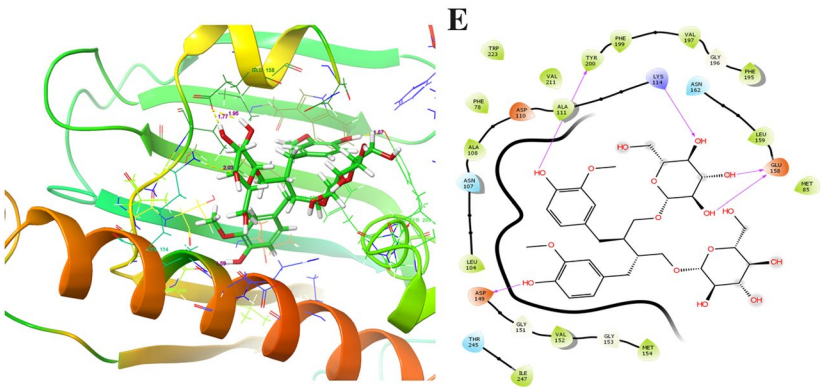

Molecular Dynamics Simulations of ligand–Protein Complexes

In order to study the dynamic behavior and the binding stability of the ligand–protein complex under suitable environmental conditions, such as temperature and pressure, MD simulations were performed for 100 ns using Desmond module of Schrodinger Biosuite. In the trajectory analysis of the backbone, RMSD for all the top lead molecules with GRP94 were stable throughout the simulation run with minimum conformational changes.

Analysis of RMSD and RMSF Plot of ZINC Ligands

The RMSD versus the simulation time was considered as a significant criterion to evaluate the stability of the dynamic behavior. The final RMSD (Root Mean Square Deviation) values of the MD simulations for the selected complexes were indicated as a time-dependent function. The RMSD trajectory analysis of the known agonist NECA (ZINC3995401) as shown in Fig. 8A displayed considerable deviations for the whole simulation time without attaining the stable state. The RMSD of ZINC72457930 complex initially showed conformational fluctuations but after 20 ns it reached the RMSD value of 2.0 Å and showed a stable interaction throughout the whole simulation process without significant deviations. Further, the trajectories of ZINC39737222 and ZINC67650204 were for the most part similar within the range of 2.0 and the dynamics of the complexes was typically more stable without much deviations. The RMSD of ZINC15669361 ligand complex displayed fluctuations initially rather attained stability after 40 ns and exhibited stability throughout the runtime of 100 ns. However, the trajectory of ZINC92952357 complex showed initial deviations from 1.0 Å and reached the stable conformation after 10 ns.

RMSF (Root Mean Square Fluctuation) plot was analyzed to evaluate the residue wise fluctuation differences in all the selected protein–ligand complex systems as well as to identify the changes in the ATP-binding region for the entire simulation period (Fig. 8B). During the entire simulations, all the protein–ligand complexes exhibited uniform fluctuations in most of the residues except significant displacement at the residues PHE199, TYR200 close to nearly 6 Å indicating considerable mobility of the residues at those regions. The overall analyses revealed that all the lead molecules that complex with GRP94 confer a similar fluctuating pattern. The interactions of ZINC39737222 revealed that residues ASP149, GLU158, ASN162, and PHE195 fluctuate at the range of 1.5 Å. Furthermore, ligands ZINC67650204, ZINC15669361, and ZINC92952357 displayed significant interactions with the following residues: ASP149, GLU158, ASN162, PHE199 as well as LYS161, ASN107, and MET154 indicating novel interactions at specifically different residues. All the five compounds exhibited similar range of fluctuations. However, ZINC72457930 showed fluctuations at majority of the amino acid residues indicating the low stability of protein–ligand interactions: THR38, TYR39, ASP34, GLU201, and THR229.

Analysis of RMSD and RMSF Plot of Selleckchem Compounds

The RMSD of *O*-Pentagalloylglucose-GRP94 complex initially exhibited conformational fluctuations but after 40 ns it reached the stable conformation with RMSD value of 3.0 Å throughout the whole simulation process without significant deviations. However, the trajectories of Eriocitrin and Secoisolariciresinol diglucoside were for the most part similar within the range of 2.4 Å and the dynamics of the complexes was typically more stable without much deviations. The RMSD of Epimedin A ligand complex displayed initial deviations from 1.0 Å rather attained stability after 20 ns with an RMSD of 3.0 Å and exhibited stability throughout the runtime of 100 ns. Conversely, the trajectory of Narcissoside complex showed considerable fluctuations throughout the runtime and finally reached stability only after 85 ns (Fig. 9A).

Table 5 Lipinski's rule and ADMET properties of top hit compounds from ZINC database

Compound ID	MW (130.0 to 725.0)	rtvFG (0–2)	Donor HB (0.0 to 6.0)	Accept HB (2.0 to 20.0)	QPlogS (− 6.5 to 0.5)	Qplo HERG (below − 5.0)	QPP Caco (< 25 poor; > 500 great)	Qplog BB (− 3.0 to − 1.2)	% of human oral absorption (> 80% is high; < 25% is poor)	Rule of three	Rule of five
ZINC39737222	405.517	0	1	7.50	− 5.122	− 5.677	823.705	− 0.826	100.00	0	0
ZINC65393724	351.45	0	1	8.00	− 2.391	− 5.108	16.350	− 0.322	52.934	0	0
ZINC40139446	390.484	0	0	4.50	− 3.849	− 5.518	97.495	− 0.940	94.439	0	0
ZINC64058574	321.421	0	0	5.75	− 3.613	− 7.234	1208.709	0.384	100.00	0	0
ZINC92952357	286.333	0	3	4.00	− 3.172	− 5.973	38.468	− 0.954	70.531	0	0
ZINC67650204	278.353	0	3	5.50	− 1.815	− 3.317	40.433	− 0.593	58.751	0	0
ZINC65432603	379.504	0	2	7.70	− 2.822	− 7.151	68.367	0.090	74.705	0	0
ZINC65393724	351.450	0	1	8.00	− 2.349	− 5.257	29.309	− 0.332	52.281	1	0
ZINC72457930	371.435	1	3	8.70	− 1.726	− 3.303	35.377	− 1.129	58.584	0	0
ZINC15669361	401.523	0	2	6.50	− 4.757	− 4.193	299.487	− 1.296	90.153	0	0

Bold values indicate the ligands that were selected for further analysis and the score based on which selection was made

Protein–Ligand Interactions

Different bonded interactions like hydrogen, hydrophobic, ionic, and water bridges are important for understanding the intermolecular recognition between the protein–ligand complexes. Among them, hydrogen bond interactions are very crucial in determining the interactive residues in the protein–ligand contacts. The histogram of all the GRP94-ligand complexes during the dynamic simulations are depicted in Fig. 9C. The results revealed that the hydrogen-bonded interactions were more prominently seen in all the five protein–ligand complexes, indicating significant maintenance of the hydrogen bonds throughout the simulation time. All the lead molecules showed stable interaction with active site residues, ASP149, GLU158, ASN162, PHE199, LYS161, and ASP107. However, Epimedin A, Narcissoside, and Eriocitrin ligands exhibited significantly higher bonded interactions than the known agonist, NECA indicating that these molecules would serve as potential agonists of GRP94 protein. However, further in vitro validations are required to confirm the theoretical predictions. Moreover, the interactions of key residues pronounced in docking studies were also retained at 100-ns MD simulations suggesting that the identified novel lead molecules would have better agonist activity than the known agonist NECA (Fig. 10).

Discussion

Disruptions in the protein-folding machinery due to protein overload leads to accumulation of misfolded proteins in the ER which activates the UPR signaling pathway to attenuate protein synthesis and maintain protein homeostasis. Within the lumen of the ER, protein chaperones assist in the folding of newly synthesized polypeptides and prevent aggregation of unfolded or misfolded proteins. Quality control exists in the ER to avoid accumulation of unfolded or misfolded proteins. Abnormal protein conformations are a major cause for disturbed cellular homeostasis; therefore, perturbations in the ER are thought to be the origin of many diseases and developmental abnormalities. Grp94, an HSP90-like protein in the ER lumen that chaperones secreted and membrane proteins, has emerged as an important target in a variety of diseases, including cancer, glaucoma, and neurodegenerative disorders, as well as viral and parasitic infections [43]. As the ER workload increases, GRP94 is transcriptionally co-regulated with other chaperones to increase the efficiency of folding and reduce the chance of misfolded proteins by preferential interactions with Grp94-dependent clients [44, 45]. Hence, therapeutic targeting of GRP94, a major ER chaperone, exploiting small molecules would enhance the efficacy of

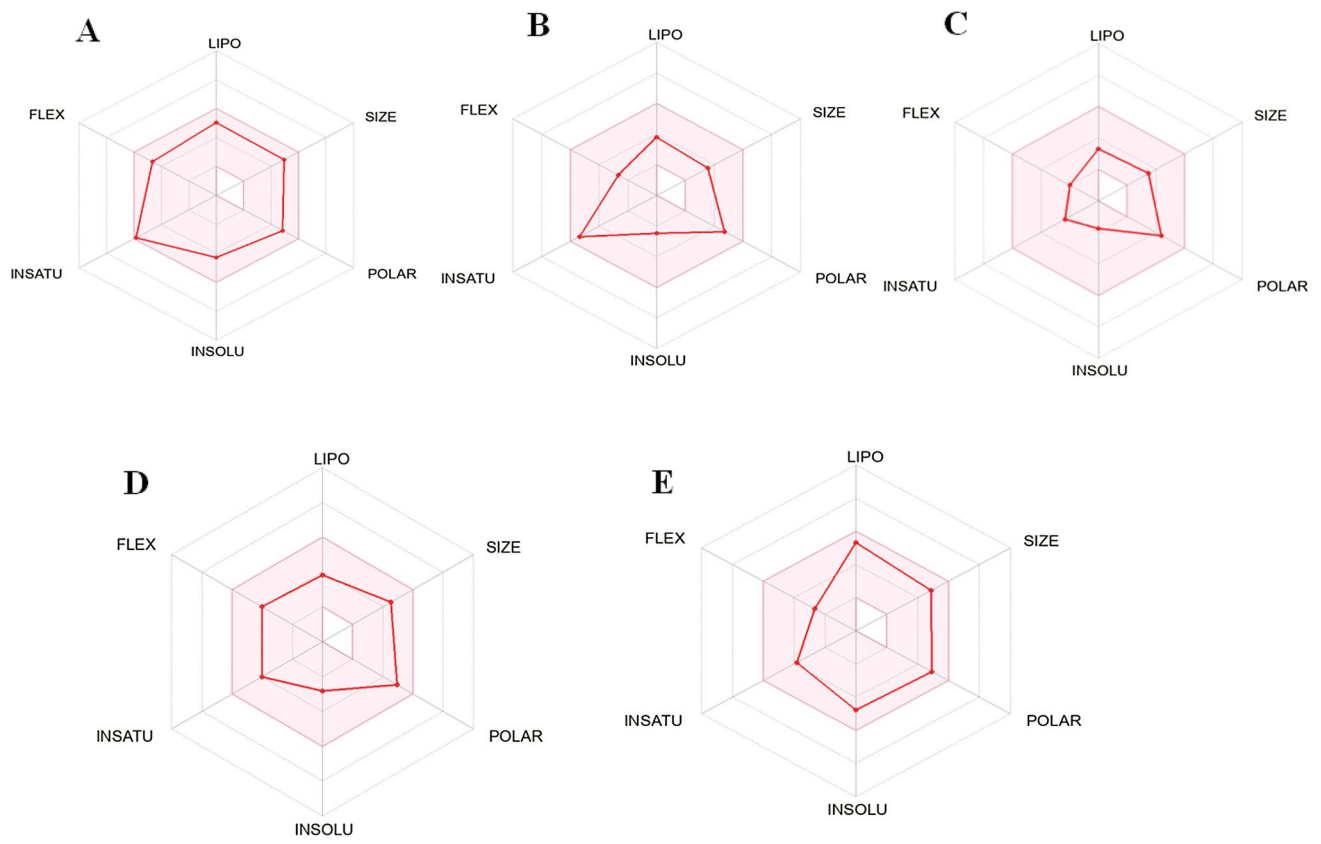

Fig. 6 SwissADME bioavailability radar showing drug likeness of different bioactive molecules—pink areas represent pharmacokinetic property, like lipophilicity, molecular weight, solubility, and flexibility. **A** ZINC39737222, **B** ZINC92952357, **C** ZINC67650204, **D** ZINC72457930, and **E** ZINC15669361

GRP94 to restore ER homeostasis and mediate cellular protection.

There is growing interest in developing new drugs that modulate Hsp90 chaperone activity. While Hsp90 inhibition has gained major attention as novel anti-cancer target, the therapeutic relevance of Hsp90 activation in other disease areas remains unexplored. Zhao et al. 2010 reported the unexpected identification of tamoxifen as an effective small-molecule activator of Hsp90 ATPase activity [46]. Natural products remain as a valuable source of small molecules that serve as potential leads for drug development. A literature survey on nature-derived ER modulators by Correia da Silva et al., 2022 listed a number of molecules notably, fisetin, withaferin, cephalostatin, and basiliolides as ER stress inducers, while hydroxytyrosol and berberine are reported to ameliorate ER stress. Several small molecules have so far been reported to modulate the different arms of the UPR and therefore exhibit promising beneficial effects in diverse human diseases. Salburinal, AA147, Apigenin, and Baicalein are different modulators that target the UPR-transducer pathways [47, 48]. Recent studies indicate that Curcumin, well-known polyphenol from turmeric, exerts antioxidant defense activity against ROS-induced myogenic cell damage via selective expression of the ER stress-inducible chaperone GRP94 [49]. GRP94 induced by curcumin maintains calcium homeostasis and protects the cell from apoptosis, demonstrating that curcumin inhibits UPR induction by inhibiting transcription factor AP-1. Consequently, this study aimed at enhancing the chaperoning activity of GRP94 through small molecule-dependent ER reprogramming to reduce the protein overload and misfolding associated with ER stress.

In this study, the selected molecule 4NH9 (Correlation between chemotype-dependent binding conformations of HSP90 alpha/beta and isoform selectivity) displays chaperone activity at the *N*-terminal regions from the residues 69–337. In addition, the NECA ligand within the 3D structure of 4NH9 binds the following actives sites ASN149, TYR200, ASN107, and ASN162 with docking score of -6.513 kcal/mol. Huck et al., 2019 reported the structural analysis of GRP94 complex with NECA revealing the interaction sites as MET85, ASN162, LEU163, THR165, ALA167, THR171, GLY196, VAL197, PHE199, and TYR200 which is adjacent to the central adenine-binding cavity of the N-terminal domain of GRP94. A

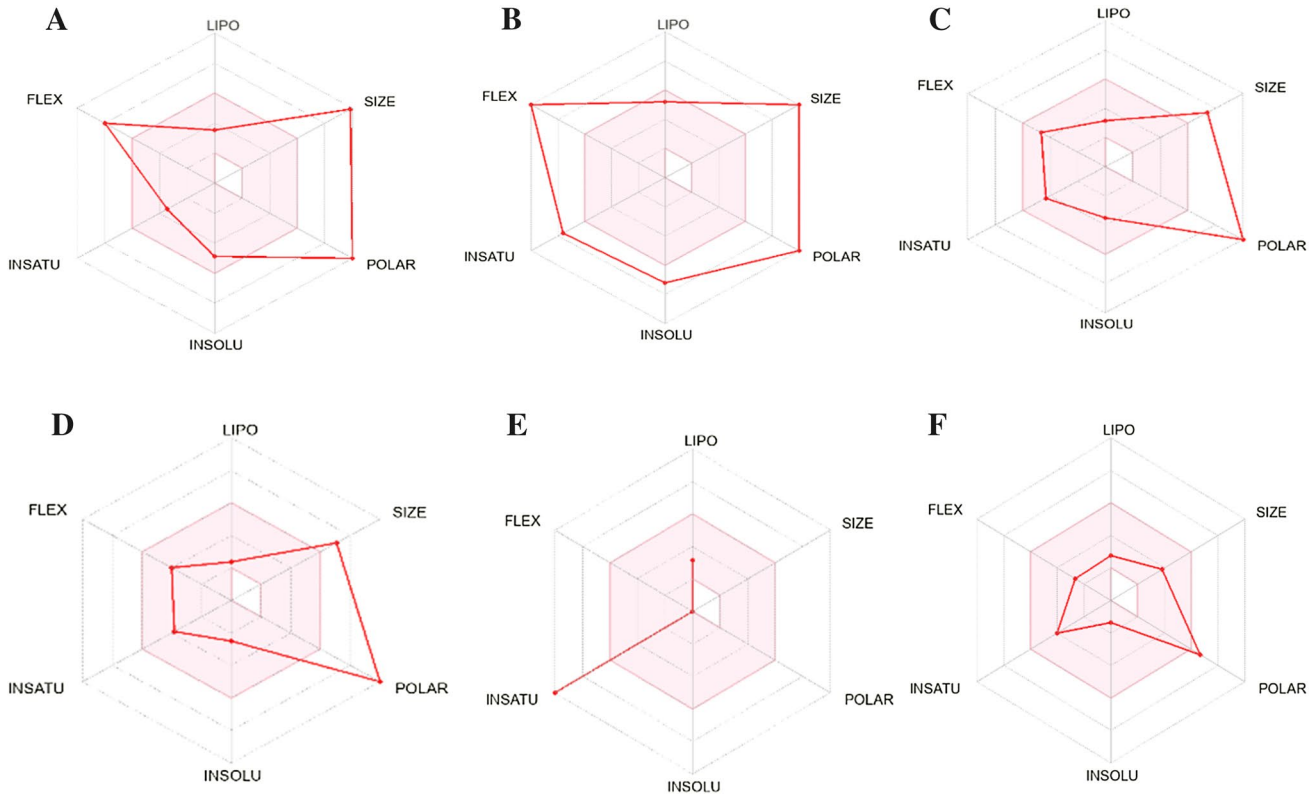

Fig. 7 SwissADME bioavailability radar showing drug likeness of different bioactive molecules—pink areas represent pharmacokinetic property, like lipophilicity, molecular weight, solubility, and flexibility. **A** Epimedin A, **B** 1,2,3,4,6-O-Pentagalloylglucose, **C** Narcissoside, **D** Eriocitrin, and **E** Secoisolariciresinol diglucoside, **F** NECA

Table 6 Drug-likeness characteristics of top hit compounds from Selleckchem database

Drug-likeness compounds	Physiochemical properties					Solubility			Pharmacokinetics	
	molecular weight (g/mol)	HB Donors	HB receptors	No. of Rotatable bonds	Consensus log P	log S (ESOL)	log S(Ali)	log S (SILICOS—IT)	GI absorption	CYP enzyme inhibitors
Epimedin A	836.83	11	19	12	− 0.41	Moderately soluble	Poorly soluble	Soluble	Low	No
Narcissoside	624.54	9	16	7	− 0.8	Soluble	Moderately soluble	Soluble	Low	No
Eriocitrin	596.53	9	15	6	− 1.3	Soluble	Soluble	Soluble	Low	No
Secoisolariciresinol diglucoside	686.70	10	16	15	− 1.14	very soluble	soluble	highly soluble	Low	No
1,2,3,4,6-O-Pentagalloylglucose	940.68	15	26	16	0.59	Poorly soluble	Insoluble	Soluble	Low	No
NECA	308.29	4	7	4	− 1.4	very soluble	very soluble	Soluble	Low	No

four-point pharmacophore model ADHR_2 was generated and 3D-QSAR analysis validated the hypothesis ADHR_2 as the best fit model with high R^2 value and least *P*-value indicative of the goodness of fit. High-throughput virtual screening of the hypothesis against Selleckchem and ZINC databases retrieved a total of 833 and 2,26,248 compounds. Using docking score, binding energy, and ADMET predictions, the following compounds ZINC39737222, ZINC92952357, ZINC67650204, ZINC72457930, and ZINC15669361 from ZINC database as well as 1,2,3,4,6-O-Pentagalloylglucose,

Epimedin A, Narcissoside, Eriocitrin, and Secoisolariciresinol diglucoside from Selleckchem library were identified as potential lead molecules. These compounds exhibited various bonded interactions with either of the active site residues in the *N*-terminal region of GRP94. All the lead compounds were within the acceptable range defined for human consumption, thereby indicating their potential as drug-like molecules. MD simulations revealed the RMSD trajectories of all complexes were stable with minor deviations within the range of 0.3 nm.

Protein–ligand interactions exhibited by the selected compounds ZINC92952357, ZINC67650204, and ZINC72457930 indicated more stable interactions with the *N*-terminal domain of GRP94 with Glide docking score from − 10.535 to − 10.454 9 kcal/mol and binding energy from − 42.559 to − 32.239 kcal/mol. Further analysis showed that these ZINC compounds are mainly piperidine and pyrazole derivatives that are known for their efficacy to differentially regulate ER stress and thus represent potential therapeutic agents to treat ER stress-related renal and neurodegenerative disorders [50]. Similarly, natural compounds such as Narcissoside, Eriocitrin, Epimedin A, and Secoisolariciresinol diglucoside showed better interactions with the ER chaperone with Glide docking score from − 13.520 to − 13.096 and glide energy from − 66.270 to − 61.039. Many natural occurring compounds including polyphenols, alkaloids, and flavonoids, target ROS and ER stress to modulate the disease pathogenesis. Narcissoside, known as narcissin, is a flavonoid derivative present in a number of medicinal plants displays several

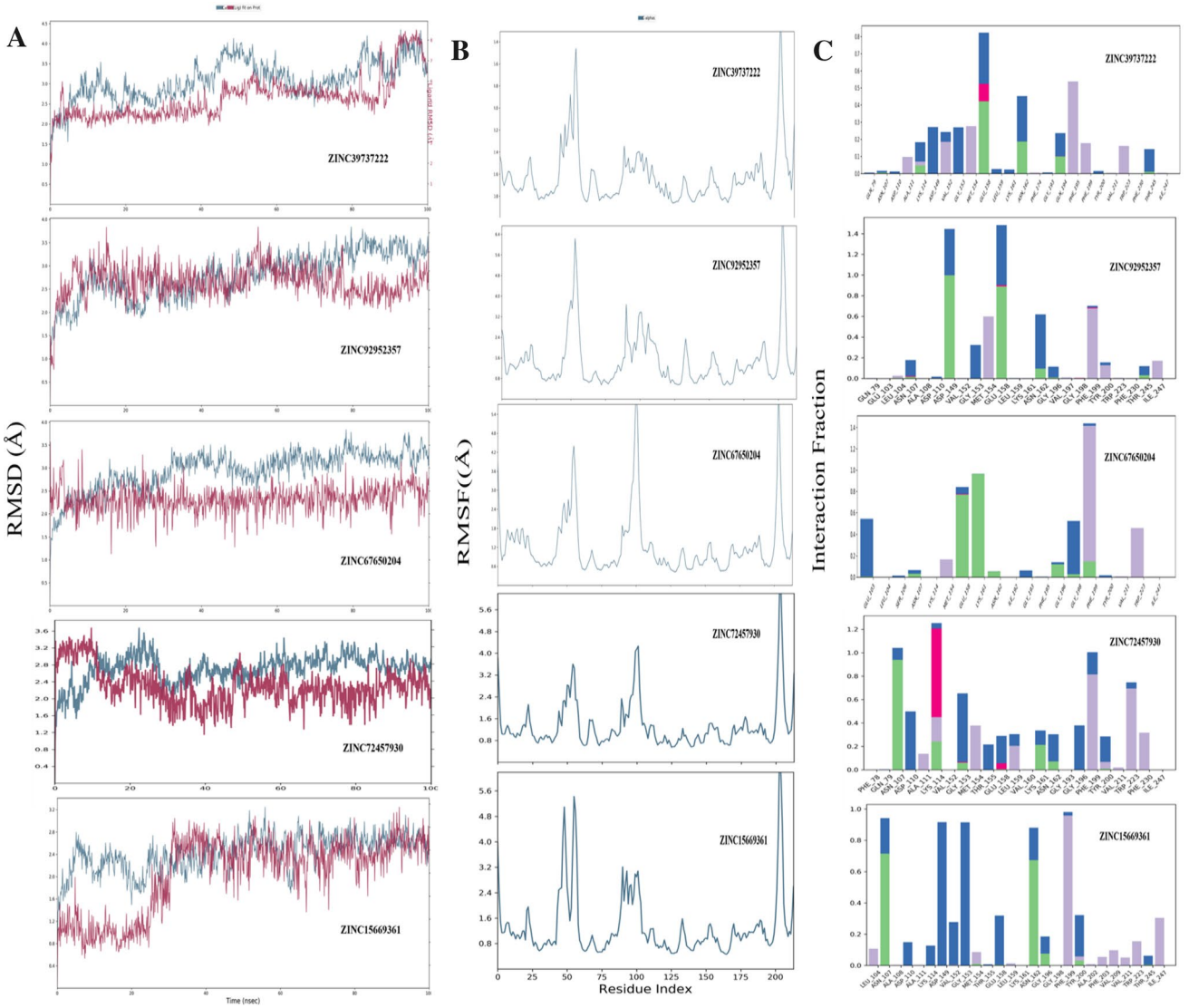

Fig. 8 MD simulations of the top hit ZINC compounds for 100 ns with RMSD, RMSF, and Interactions

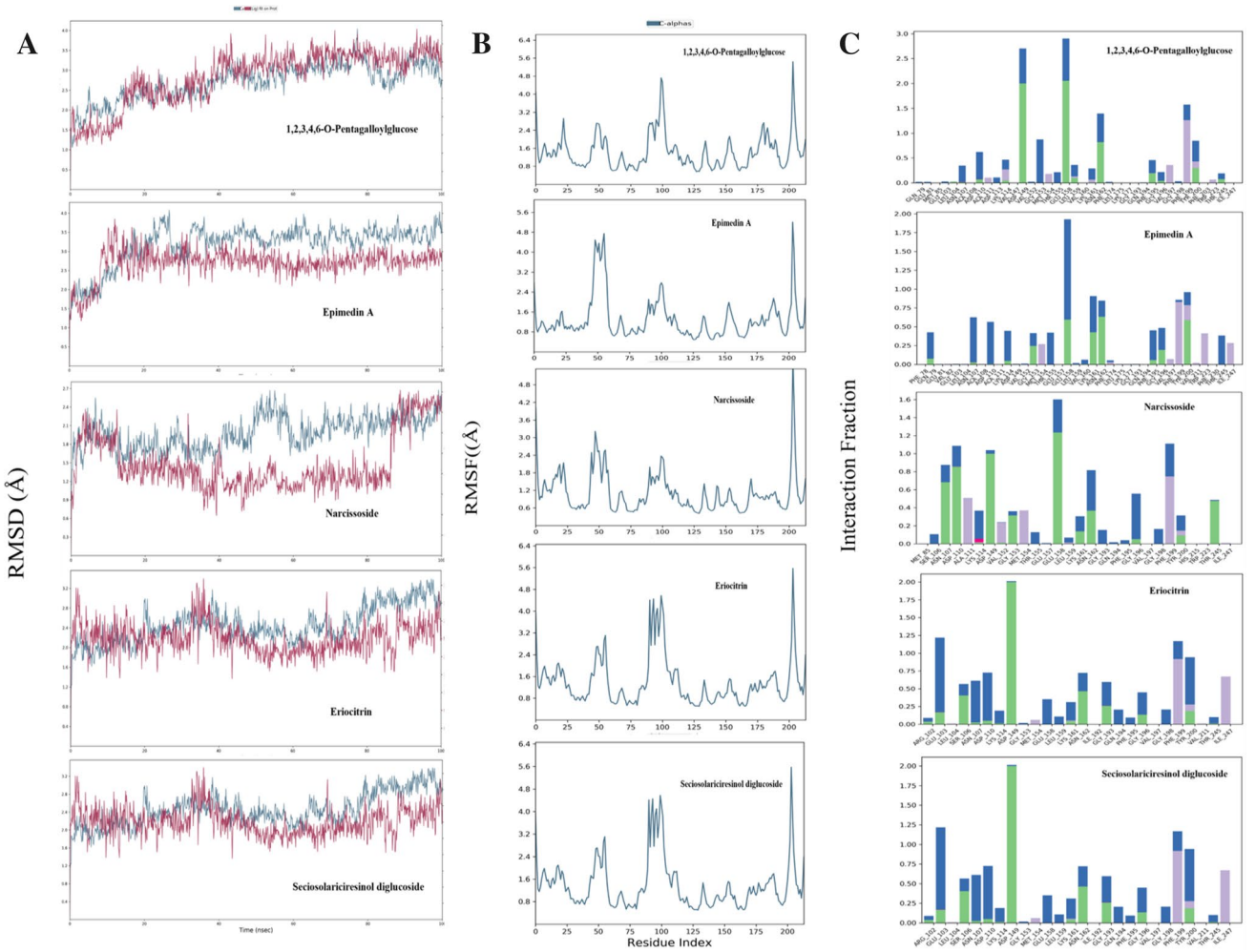

Fig. 9 MD simulations of the top hit Selleckchem compounds for 100 ns with RMSD, RMSF, and Interactions

pharmacological properties. It exhibits neuroprotective potential by preventing the ROS-induced oxidative stress and apoptosis [51]. Eriocitrin, a major flavonoid in citrus plants, has displayed suppressive effect on oxidative stress and lipid-lowering effect in rats [52]. Secoisolariciresinol diglucoside, a lignan found mainly in flaxseed, has significantly regulated the lipid metabolic disorders through the ER stress-Ca^{2+}-mitochondrial-associated pathway [53]. However, the mechanism of regulation of these natural compounds on ER chaperones as well as UPR pathway are yet to be elucidated in wet lab studies.

Conclusion

In the present study, novel GRP94 agonists were designed by means of core hopping approach and the newly designed scaffolds of NECA were subjected to pharmacophore hypothesis testing, 3D-QSAR model validations, and high-throughput virtual screening on ZINC and Selleckchem databases to effectively identify small molecules for enhancing GRP94 activity. The screened compounds were validated as effective drug molecules based on ADMET prediction and the top lead compounds were subjected to MD simulations to study the binding stability of the protein–ligand complex. The study yielded 10 top-docked compounds, which were then filtered further using post-docking analysis (top 5). Significantly, Epimedin A, Narcissoside, Eriocitrin, and ZINC92952357, ZINC67650204, and ZINC72457930 satisfy all the parameters investigated, such as docking score, binding energy, ADMET properties, and dynamic simulations. The present study deciphers that core hopping coupled with atom-based 3D-QSAR model and docking studies helped in designing analogs with better activity that may serve as potent small-molecule agonists for GRP94 to alleviate ER stress-associated disease pathogenesis. However, further

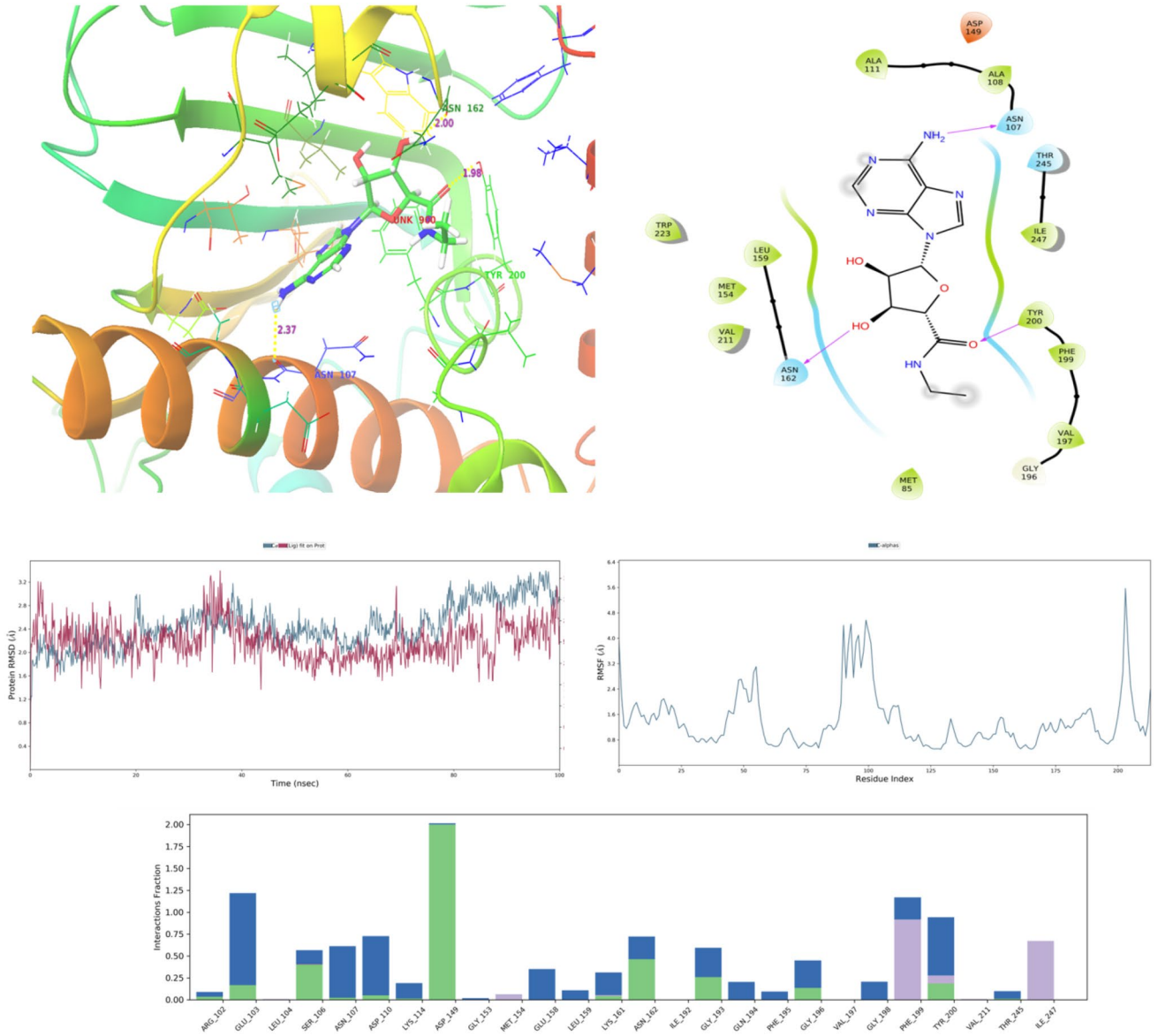

Fig. 10 Binding interactions and MD simulations of the known agonist NECA (ZINC3995401) with RMSD and RMSF

experimental validations are required to substantiate the efficacy of these small molecules.

Funding The authors are grateful to Department of Biotechnology (DBT), Ministry of Science and Technology, New Delhi, India for providing the necessary research support to carry out this study (Ref: BT/PR30828/MED/97/434/2018 dated 26.09.2019).

Declarations

Conflict of interest The authors declare that they have no conflict of interest.

Ethical approval This article does not contain any studies with human participants or animals performed by any of the authors.

References

1. Hetz, C. (2012). The unfolded protein response: Controlling cell fate decisions under ER stress and beyond. *Nature Reviews Molecular Cell Biology, 13*(2), 89–102. https://doi.org/10.1038/nrm3270
2. Yoo, Y. S., Han, H. G., & Jeon, Y. J. (2017). Unfolded protein response of the endoplasmic reticulum in tumor progression and immunogenicity. *Oxidative Medicine and Cellular Longevity, 2017*, 2969271. https://doi.org/10.1155/2017/2969271
3. Ni, M., & Lee, A. S. (2007). ER chaperones in mammalian development and human diseases. *FEBS Letters, 581*(19), 3641–3651. https://doi.org/10.1016/j.febslet.2007.04.045
4. Schönthal, A. H. (2012). Endoplasmic reticulum stress: Its role in disease and novel prospects for therapy. *Scientifica (Cairo)*. https://doi.org/10.6064/2012/857516

5. Calamini, B., & Morimoto, R. I. (2012). Protein homeostasis as a therapeutic target for diseases of protein conformation. *Current Topics in Medicinal Chemistry, 12*(22), 2623–2640. https://doi.org/10.2174/1568026611212220014
6. Gestwicki, J. E., & Garza, D. (2012). Protein quality control in neurodegenerative disease. *Progress in Molecular Biology and Translational Science, 107*, 327–353. https://doi.org/10.1016/B978-0-12-385883-2.00003-5
7. Chen, J. J., Genereux, J. C., & Wiseman, R. L. (2015). Endoplasmic reticulum quality control and systemic amyloid disease: Impacting protein stability from the inside out. *IUBMB Life, 67*(6), 404–413. https://doi.org/10.1002/iub.1386
8. Plate, L., Cooley, C. B., Chen, J. J., Paxman, R. J., Gallagher, C. M., Madoux, F., Genereux, J. C., Dobbs, W., Garza, D., Spicer, T. P., Scampavia, L., Brown, S. J., Rosen, H., Powers, E. T., Walter, P., Hodder, P., Wiseman, R. L., & Kelly, J. W. (2016). Small molecule proteostasis regulators that reprogram the ER to reduce extracellular protein aggregation. *eLife, 5*, e15550. https://doi.org/10.7554/eLife.15550
9. Almanza, A., Carlesso, A., Chintha, C., Creedican, S., Doultsinos, D., Leuzzi, B., Luís, A., McCarthy, N., Montibeller, L., More, S., Papaioannou, A., Püschel, F., Sassano, M. L., Skoko, J., Agostinis, P., de Belleroche, J., Eriksson, L. A., Fulda, S., Gorman, A. M., … Samali, A. (2019). Endoplasmic reticulum stress signaling—from basic mechanisms to clinical applications. *FEBS Journal, 286*(2), 241–278. https://doi.org/10.1111/febs.14608
10. Peng, C., Zhao, F., Li, H., Li, L., Yang, Y., & Liu, F. (2022). HSP90 mediates the connection of multiple programmed cell death in diseases. *Cell Death & Disease, 13*(11), 929. https://doi.org/10.1038/s41419-022-05373-9
11. Halperin, L., Jung, J., & Michalak, M. (2014). The many functions of the endoplasmic reticulum chaperones and folding enzymes. *IUBMB Life, 66*, 318–326. https://doi.org/10.1002/iub.1272
12. Ozcan, L., & Tabas, I. (2012). Role of endoplasmic reticulum stress in metabolic disease and other disorders. *Annual Review of Medicine, 63*, 317–328. https://doi.org/10.1146/annurev-med-043010-144749
13. Argon, Y., & Simen, B. B. (1999). GRP94, an ER chaperone with protein and peptide binding properties. *Seminars in Cell & Developmental Biology, 10*(5), 495–505. https://doi.org/10.1006/scdb.1999.0320
14. Eletto, D., Dersh, D., & Argon, Y. (2010). GRP94 in ER quality control and stress responses. *Seminars in Cell & Developmental Biology, 21*(5), 479–485. https://doi.org/10.1016/j.semcdb.2010.03.004
15. Amankwah, Y. S., Collins, P., Fleifil, Y., Unruh, E., Ruiz Márquez, K. J., Vitou, K., & Kravats, A. N. (2022). Grp94 works upstream of BiP in protein remodeling under heat stress. *Journal of Molecular Biology, 434*(19), 167762. https://doi.org/10.1016/j.jmb.2022.167762
16. Huck, J. D., Que, N. L., Immormino, R. M., Shrestha, L., Taldone, T., Chiosis, G., & Gewirth, D. T. (2019). NECA derivatives exploit the paralog-specific properties of the site 3 side pocket of Grp94, the endoplasmic reticulum Hsp90. *Journal of Biological Chemistry, 294*(44), 16010–16019.
17. Soldano, K. L., Jivan, A., Nicchitta, C. V., & Gewirth, D. T. (2003). Structure of the N-terminal domain of GRP94: Basis for ligand specificity and regulation. *Journal of Biological Chemistry, 278*(48), 48330–48338.
18. Grandjean, J. M. D., & Wiseman, R. L. (2020). Small molecule strategies to harness the unfolded protein response: Where do we go from here? *Journal of Biological Chemistry, 295*(46), 15692–15711. https://doi.org/10.1074/jbc.REV120.010218
19. Gonzalez-Teuber, V., Albert-Gasco, H., Auyeung, V. C., Papa, F. R., Mallucci, G. R., & Hetz, C. (2019). Small molecules to improve ER proteostasis in disease. *Trends in Pharmacological Sciences, 40*(9), 684–695. https://doi.org/10.1016/j.tips.2019.07.003
20. Ernst, J. T., Liu, M., Zuccola, H., Neubert, T., Beaumont, K., Turnbull, A., Kallel, A., Vought, B., & Stamos, D. (2014). Correlation between chemotype-dependent binding conformations of HSP90α/β and isoform selectivity-Implications for the structure-based design of HSP90α/β selective inhibitors for treating neurodegenerative diseases. *Bioorganic & Medicinal Chemistry Letters, 24*(1), 204–208. https://doi.org/10.1016/j.bmcl.2013.11.036
21. Schrödinger (2018) LigPrep. Schrödinger, LLC, New York
22. Harder, E., Damm, W., Maple, J., Wu, C., Reboul, M., Xiang, J. Y., Wang, L., Lupyan, D., Dahlgren, M. K., Knight, J. L., Kaus, J. W., Cerutti, D. S., Krilov, G., Jorgensen, W. L., Abel, R., & Friesner, R. A. (2016). OPLS3: A Force field providing broad coverage of drug-like small molecules and proteins. *Journal of Chemical Theory and Computation, 12*(1), 281–296. https://doi.org/10.1021/acs.jctc.5b00864
23. Wang, X. J., Zhang, J., Wang, S. Q., Xu, W. R., Cheng, X. C., & Wang, R. L. (2014). Identification of novel multitargeted PPARα/γ/δ pan agonists by core hopping of rosiglitazone. *Drug Design Development and Therapy, 8*, 2255–2262. https://doi.org/10.2147/DDDT.S70383
24. Li, W. Y., Ma, Y., Li, H. X., Lu, X. H., Du, S., Ma, Y. C., Zhou, L., & Wang, R. L. (2020). Scaffold-based selective SHP2 inhibitors design using core hopping, molecular docking, biological evaluation and molecular simulation. *Bioorganic Chemistry, 105*, 104391. https://doi.org/10.1016/j.bioorg.2020.104391
25. Dixon, S. L., Smondyrev, A. M., Knoll, E. H., Rao, S. N., Shaw, D. E., & Friesner, R. A. (2006). PHASE: A new engine for pharmacophore perception, 3D QSAR model development, and 3D database screening: 1. Methodology and preliminary results. *Journal of Computer Aided Molecular Design, 20*(10–11), 647–671. https://doi.org/10.1007/s10822-006-9087-6
26. Vanajothi, R., Hemamalini, V., Jeyakanthan, J., & Premkumar, K. (2020). Ligand-based pharmacophore mapping and virtual screening for identification of potential discoidin domain receptor 1 inhibitors. *Journal of Biomolecular Structure Dynamics, 38*(9), 2800–2808. https://doi.org/10.1080/07391102.2019.1640132
27. Ding, Y. L., Lyu, Y. C., & Leong, M. K. (2017). In silico prediction of the mutagenicity of nitroaromatic compounds using a novel two-QSAR approach. *Toxicology In Vitro, 40*, 102–114. https://doi.org/10.1016/j.tiv.2016.12.013
28. Drwal, M. N., & Griffith, R. (2013). Combination of ligand- and structure-based methods in virtual screening. *Drug Discovery Today Technologies, 10*(3), e395-401. https://doi.org/10.1016/j.ddtec.2013.02.002
29. Wang, Y., Feng, S., Gao, H., & Wang, J. (2020). Computational investigations of gram-negative bacteria phosphopantetheine adenylyltransferase inhibitors using 3D-QSAR, molecular docking and molecular dynamic simulations. *Journal of Biomolecular Structure Dynamics, 38*(5), 1435–1447. https://doi.org/10.1080/07391102.2019.1608305
30. Koes, D. R., & Camacho, C. J. (2012). ZINCPharmer: pharmacophore search of the ZINC database. *Nucleic Acids Research, 40*(Web Server issue), W409–W414. https://doi.org/10.1093/nar/gks378
31. Koes, D. R., Pabon, N. A., Deng, X., Phillips, M. A., & Camacho, C. J. (2015). A Teach-discover-treat application of zincpharmer: an online interactive pharmacophore modeling and virtual screening tool. *PLoS ONE, 10*(8), e0134697. https://doi.org/10.1371/journal.pone.0134697
32. Friesner, R. A., Murphy, R. B., Repasky, M. P., Frye, L. L., Greenwood, J. R., Halgren, T. A., Sanschagrin, P. C., & Mainz, D. T. (2006). Extra precision glide: docking and scoring incorporating a model of hydrophobic enclosure for protein-ligand

complexes. *Journal of Medicinal Chemistry, 49*(21), 6177–6196. https://doi.org/10.1021/jm051256o
33. Ntie-Kang, F. (2013). An in silico evaluation of the ADMET profile of the StreptomeDB database. *Springerplus, 30*(2), 353. https://doi.org/10.1186/2193-1801-2-353
34. Lipinski, C. A., Lombardo, F., Dominy, B. W., & Feeney, P. J. (2001). Experimental and computational approaches to estimate solubility and permeability in drug discovery and development settings. *Advanced Drug Delivery Reviews, 46*(1–3), 3–26. https://doi.org/10.1016/s0169-409x(00)00129-0
35. Daina, A., Michielin, O., & Zoete, V. (2017). SwissADME: A free web tool to evaluate pharmacokinetics, drug-likeness and medicinal chemistry friendliness of small molecules. *Science and Reports, 7*, 42717. https://doi.org/10.1038/srep42717
36. Jorgensen, W. L., Maxwell, D. S., & Tirado-Rives, J. (1996). Development and testing of the OPLS all-atom force field on conformational energetics and properties of organic liquids. *Journal of the American Chemical Society, 118*(45), 11225–11236.
37. Mohankumar, T., Chandramohan, V., Lalithamba, H. S., Jayaraj, R. L., Kumaradhas, P., Sivanandam, M., & Elangovan, N. (2020). Design and molecular dynamic investigations of 7, 8-dihydroxyflavone derivatives as potential neuroprotective agents against alpha-synuclein. *Scientific Reports, 10*(1), 1–10.
38. Singh, K., & Muthusamy, K. (2013). Molecular modeling, quantum polarized ligand docking and structure-based 3D-QSAR analysis of the imidazole series as dual AT1 and ETA receptor antagonists. *Acta Pharmacologica Sinica, 34*, 1592–1606. https://doi.org/10.1038/aps.2013.129
39. Pasala, C., Katari, S. K., Nalamolu, R. M., Aparna, R. B., & Amineni, U. (2019). Integration of core hopping, quantum-mechanics, molecular mechanics coupled binding-energy estimations and dynamic simulations for fragment-based novel therapeutic scaffolds against Helicobacter pylori strains. *Computational Biology and Chemistry*. https://doi.org/10.1016/j.compbiolchem
40. Bhansali, S., & Kulkarni, V. M. (2014). Pharmacophore generation, atom-based 3D-QSAR, docking, and virtual screening studies of p38-α mitogen activated protein kinase inhibitors: pyridopyridazin-6-ones (part Research and Reports in Medicinal Chemistry). *Research and Reports in Medicinal Chemistry, 4*, 1–21.
41. Rodríguez, D., Gao, Z. G., Moss, S. M., Jacobson, K. A., & Carlsson, J. (2015). Molecular docking screening using agonist-bound GPCR structures: Probing the A2A adenosine receptor. *Journal of Chemical Information and Modeling, 55*(3), 550–563. https://doi.org/10.1021/ci500639g
42. Mishra, S., & Dahima, R. (2019). In vitro ADME studies of TUG-891, a GPR-120 inhibitor using SwissADME predictor. *Journal of Drug Delivery Therapeutics, 9*, 366–369. https://doi.org/10.22270/JDDT.V9I2-S.2710
43. Tosh, D. K., Brackett, C. M., Jung, Y. H., Gao, Z. G., Banerjee, M., Blagg, B. S. J., & Jacobson, K. A. (2021). Biological Evaluation of 5'-(N-Ethylcarboxamido)adenosine analogues as Grp94-selective inhibitors. *ACS Medicinal Chemistry Letters, 12*(3), 373–379. https://doi.org/10.1021/acsmedchemlett.0c00509
44. Marzec, M., Eletto, D., & Argon, Y. (2012). GRP94: An HSP90-like protein specialized for protein folding and quality control in the endoplasmic reticulum. *Biochimica et Biophysica Acta, 1823*(3), 774–787. https://doi.org/10.1016/j.bbamcr.2011.10.013
45. Wassenberg, J. J., Reed, R. C., & Nicchitta, C. V. (2000). Ligand interactions in the adenosine nucleotide-binding domain of the Hsp90 chaperone, GRP94. II. Ligand-mediated activation of GRP94 molecular chaperone and peptide binding activity. *Journal of Biological Chemistry, 275*(30), 22806–22814. https://doi.org/10.1074/jbc.M001476200
46. Zhao, R., Leung, E., Grüner, S., Schapira, M., & Houry, W. A. (2010). Tamoxifen enhances the Hsp90 molecular chaperone ATPase activity. *PLoS ONE, 5*(4), e9934. https://doi.org/10.1371/journal.pone.0009934
47. Liu, H., Yang, J., Li, L., Shi, W., Yuan, X., & Wu, L. (2016). The natural occurring compounds targeting endoplasmic reticulum stress. *Evid Based Complement Alternat Med., 2016*, 7831282. https://doi.org/10.1155/2016/7831282
48. da Correia, S. D., Valentão, P., Andrade, P. B., & Pereira, D. M. (2022). A Pipeline for natural small molecule inhibitors of endoplasmic reticulum stress. *Frontiers in Pharmacology, 13*, 956154. https://doi.org/10.3389/fphar.2022.956154
49. Conn, P. Michael. (2011). The Unfolded Protein Response and Cellular Stress Part C. In: Inagi, R. (eds), Inhibitors of Advanced Glycation and Endoplasmic Reticulum Stress, (1st ed., 20:361–377). San Diego, Academic Press, an imprint of Elsevier
50. Hammad, A. S., Ravindran, S., Khalil, A., & Munusamy, S. (2017). Structure-activity relationship of piperine and its synthetic amide analogs for therapeutic potential to prevent experimentally induced ER stress in vitro. *Cell Stress and Chaperones, 22*(3), 417–428. https://doi.org/10.1007/s12192-017-0786-9
51. Fu, R. H., Tsai, C. W., Liu, S. P., Chiu, S. C., Chen, Y. C., Chiang, Y. T., Kuo, Y. H., Shyu, W. C., & Lin, S. Z. (2022). Neuroprotective capability of narcissoside in 6-OHDA-exposed Parkinson's disease Models through enhancing the MiR200a/Nrf-2/GSH axis and mediating MAPK/Akt associated signaling pathway. *Antioxidants (Basel)., 11*(11), 2089. https://doi.org/10.3390/antiox11112089
52. Hiramitsu, M., Shimada, Y., Kuroyanagi, J., Inoue, T., Katagiri, T., Zang, L., Nishimura, Y., Nishimura, N., & Tanaka, T. (2014). Eriocitrin ameliorates diet-induced hepatic steatosis with activation of mitochondrial biogenesis. *Science and Reports, 15*(4), 3708. https://doi.org/10.1038/srep03708
53. Wei, L., Zhao, C., Dong, S., Yao, S., Ji, B., Zhao, B., Liu, Z., Liu, X., & Wang, Y. (2020). Secoisolariciresinol diglucoside alleviates hepatic lipid metabolic misalignment involving the endoplasmic reticulum-mitochondrial axis. *Food & Function, 11*(5), 3952–3963. https://doi.org/10.1039/d0fo00124d